Journal of
Materials in Life Sciences

Vol. 4 No. 1 (2025)

Full Paper

Synthesis and Characterization of MIL-100(Fe) Metal-Organic Framework on Titania as Visible Light-Active Photocatalyst for Bisphenol A Degradation

Elis Osman[a], Sheela Chandren[a,b]*

[a]Department of Chemistry, Faculty of Science, Universiti Teknologi Malaysia, 81310 UTM Johor Bahru, Johor, Malaysia.

[b]Centre for Sustainable Nanomaterials, Universiti Teknologi Malaysia, 81310 UTM Johor Bahru, Johor, Malaysia.

Article history
Received
19 March 2025
Revised
09 May 2025
Accepted
26 May 2025
Published online
31 May 2025

*Corresponding author
sheela@utm.my

Abstract

Titania (TiO_2) is a widely utilized metal oxide nanomaterial used for pollutant degradation; however, its limited activity under visible light restricts its broader photocatalytic applications. In this study, TiO_2 was incorporated with a metal-organic framework, MIL-100(Fe), via the hydrothermal synthesis route, forming MIL-100(Fe)/TiO_2 composites. This study also investigated the impact of TiO_2 loadings in MIL-100(Fe)/TiO_2 composites. The synthesized composites were analyzed for their structural features and optical characteristics using various characterization methods. X-ray diffraction (XRD) confirmed the presence of both anatase and rutile TiO_2 phases, while Fourier transform infrared (FTIR) spectroscopy validated the key functional groups. Ultraviolet-visible near-infrared (UV-Vis-NIR) spectroscopy revealed that MIL-100(Fe)/TiO_2 composites with 5.4 mmol of TiO_2 (MIL-100(Fe)/TiO_2 (5.4)) exhibited a reduced bandgap of 1.70 eV, compared to 2.10 eV for MIL-100(Fe)/TiO_2 composites with 1.8 mmol of TiO_2 (MIL-100(Fe)/TiO_2 (1.8)), enhancing visible-light absorption. Field emission scanning electron microscopy (FESEM) revealed particle sizes ranging from 74.7 to 99.1 nm. The photocatalytic performance of the synthesized MIL-100(Fe)/TiO_2 composites was tested by monitoring the degradation of bisphenol A (BPA) under UV light exposure. Notably, the synthesized MIL-100(Fe)/TiO_2 (5.4) attained the highest photocatalytic activity (81.43%), while MIL-100(Fe)/TiO_2 (1.8) showed the lowest efficiency (36.36%). Given the improved visible-light absorption from the reduced bandgap, further evaluation under visible-light conditions was conducted. The results revealed that MIL-100(Fe)/TiO_2 (5.4) achieved significant degradation (69.49%), whereas commercial TiO_2 exhibited no activity (0%). These findings confirm that MIL-100(Fe)/TiO_2 composites enhance visible-light-driven photocatalysis by extending light absorption and improving charge separation, thereby reducing electron-hole recombination for effective environmental remediation.

Keywords *titania, metal-organic framework, photocatalysis, bisphenol A*

1.0 INTRODUCTION

Titania (TiO_2), a metal oxide, is an essential semiconductor material that has garnered extensive attention for its photocatalytic properties [1]. As a photocatalyst, TiO_2 is highly effective in degrading both organic and inorganic pollutants, making it a key material for addressing environmental pollution. TiO_2 occurs in three crystalline phases: anatase, rutile, and brookite, with anatase showing the highest photocatalytic activity [2]. Its broad application is due to its high chemical and thermal stability, low toxicity, affordability, and multifunctionality which allow its application in a variety of fields, including environmental remediation, energy production, and material science [3].

Photocatalytic activity of TiO_2 is mainly triggered under ultraviolet (UV) light due to its wide bandgap (E_g ~3.2 eV), enabling the absorption of high-energy photons [4]. This band structure enables TiO_2 to absorb only high-energy UV photons, leading to the excitation of electrons initially located in the valence band (VB) to the conduction band (CB), thus generating electron-hole pairs that facilitate oxidation-reduction reactions. Despite its remarkable photocatalytic potential, TiO_2's absorption is limited to the UV range, which comprises approximately only 5% of solar radiation, restricting its efficiency under solar irradiation [5]. In addition, the rapid recombination of photoinduced charge carriers further reduces the efficiency of pollutant degradation, posing a major challenge in environmental remediation and water purification technologies [6].

Numerous strategies have been developed to enhance the photocatalytic performance of TiO_2. Common techniques include doping with metals and non-metals, as well as surface modification using polymers [7]. Metal doping, such as with platinum (Pt), gold (Au), and silver (Ag), can help extend TiO_2's absorption into the visible light range, but these metals are often expensive and may introduce new recombination centres. Non-metal doping, such as with carbon (C), nitrogen (N), and sulphur (S), aims to lower the E_g, but the effectiveness of these materials in reducing charge recombination remains limited [8].

In order to overcome the aforementioned limitations, this study proposes modifying TiO_2 with metal-organic frameworks (MOFs) to form heterojunctions, a strategy that offers an environmentally friendly and versatile approach to enhancing TiO_2's photocatalytic properties. Among various MOFs, MIL-100(Fe) has attracted considerable interest due to its mesoporous structure, high surface area, and robust thermal and chemical stability [9]. Moreover, its photoactive Fe centers and porous framework can significantly facilitate charge separation and improve light absorption [10]. Integrating MIL-100(Fe) with TiO_2 can potentially overcome TiO_2's UV-limited activation, reduce electron-hole recombination, and improve photocatalytic performance under both UV and visible light [11].

Earlier studies have shown that MIL-100(Fe)/TiO_2 composites can be synthesized using an iron precursor, trimesic acid (H_3BTC), and other reagents [12]. Several synthesis methods have been explored, including co-precipitation, self-assembly, and hydrothermal techniques. Among these, the hydrothermal method is preferred due to its environmental friendliness, ability to produce high-purity crystalline materials, and ease of scale-up. This method, which operates under sealed conditions using aqueous solvents, also offers the potential for scaling up and maintaining reproducibility.

In this study, MIL-100(Fe)/TiO_2 composites were synthesized using a hydrothermal route with varying TiO_2 contents. The resulting materials were assessed for their ability to degrade bisphenol A (BPA) under both ultraviolet and visible light irradiations. BPA is a toxic environmental contaminant commonly found in plastic products and industrial wastewater [13], and has garnered significant attention due to its endocrine-disrupting properties, which pose serious health risks to humans and wildlife. Its persistence and bioaccumulation in aquatic ecosystems further exacerbate environmental contamination, necessitating immediate and effective remediation strategies [14]. Therefore, developing advanced photocatalysts for BPA degradation is crucial. Subsequently, the composites exhibiting the highest and lowest degradation efficiency were selected for detailed physicochemical characterization, followed by BPA degradation in different pH utilizing the MIL-100(Fe)/TiO_2 composites optimized for TiO_2 content to evaluate the optimum pH condition for BPA degradation.

2.0 Materials and Methods

2.1 Materials

The following analytical-grade chemicals were used without any further purification: iron(III) chloride hexahydrate ($FeCl_3{\cdot}6H_2O$), sodium carbonate (Na_2CO_3), titanium(IV) oxide (TiO_2), hydrochloric acid (HCl), sodium hydroxide (NaOH), trimesic acid (H_3BTC), ethanol, and bisphenol A (BPA). Distilled water served as the primary solvent throughout all synthesis and washing procedures. All reagents were obtained from Aldrich.

2.2 Preparation of MIL-100(Fe)/TiO_2 Composites

The MIL-100(Fe)/TiO_2 composites were prepared via a hydrothermal route by varying the amount of TiO_2 (1.8, 3.6, 5.4, and 7.2 mmol), in accordance with previous studies suggesting improved photocatalytic performance at specific loadings [15]. A homogeneous solution was prepared by dissolving H_3BTC (12 mmol), Na_2CO_3 (25 mmol), $FeCl_3{\cdot}6H_2O$ (18 mmol) and dispersing TiO_2 in 36 mL of distilled water. The solution was placed in a stainless-steel autoclave lined with Teflon and subjected to a hydrothermal process at 160 °C for 12 h. Once cooled to room temperature, the resulting light orange solid was separated via centrifugation. The solid product was repeatedly washed, initially with distilled water to remove soluble impurities, and then, with hot ethanol to remove residual H_3BTC from the surface and pores. The purified material was subsequently dried overnight at 60 °C. The optimal TiO_2 content for the MIL-100(Fe)/TiO_2 composite was determined based on the photodegradation efficiency of BPA under UV irradiation. Details on the sample coding for each synthesized composite are provided in Table 1.

Table 1: Coding of MIL-100(Fe)/TiO_2 composites prepared

Sample code	TiO_2 (mmol)	$FeCl_3 \cdot 6H_2O$ (mmol)	H_3BTC (mmol)	Na_2CO_3 (mmol)
MIL-100(Fe)/TiO_2 (1.8)	1.8	18	12	25
MIL-100(Fe)/TiO_2 (3.6)	3.6	18	12	25
MIL-100(Fe)/TiO_2(5.4)	5.4	18	12	25
MIL-100(Fe)/TiO_2 (7.2)	7.2	18	12	25

2.3 Characterization

MIL-100(Fe)/TiO_2 composites underwent comprehensive characterization using advanced techniques. Fourier-transform infrared (FTIR) spectroscopy, performed on a Perkin-Elmer 1600 spectrometer, was used for identifying functional groups in the samples. Optical properties and bandgap energies were examined using UV-Vis-NIR spectroscopy with a JASCO V-670 spectrophotometer. Surface morphology and particle size distribution were investigated through field-emission scanning electron microscopy (FESEM) on a JEOL JSM-6701F instrument operated at 5.0 kV. The crystalline phases present in the composites were determined by X-ray diffraction (XRD) analysis using a Bruker D8 Advance diffractometer.

2.4 Photocatalytic Testing

The efficiency of the MIL-100(Fe)/TiO_2 composites in photocatalytic degradation was evaluated by tracking the breakdown of BPA under ultraviolet light emitted from a 6 W lamp, following a method adapted from Rojas-Guerrero *et al.* [16]. BPA at a concentration of 25 ppm was combined with 0.05 g of MIL-100(Fe)/TiO_2 composites before being subjected to this test. The suspension was vigorously stirred at 800 rpm using a magnetic stirrer and maintained in the dark within a chamber equipped with a Philips 18 W LED bulb for 1 h to allow the system to reach equilibrium. Following this period, the sample was exposed to light irradiation, and after 3.5 h, the BPA concentration was measured using a UV-Vis spectrophotometer. The apparatus used in the photocatalytic reaction is shown in Figure 1. The degradation percentage was calculated using Equation 1.

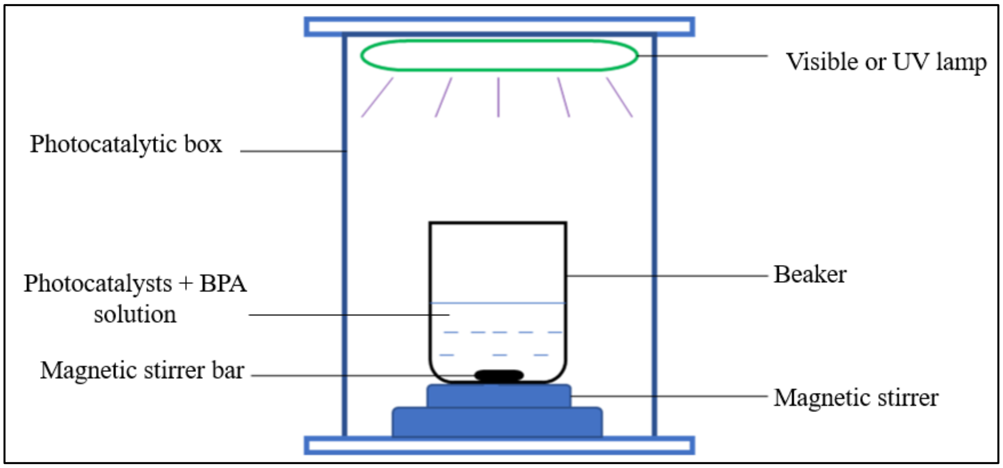

Figure 1: Set up for the photocatalytic reaction.

$$\text{Degradation percentage (\%)} = \frac{C_o - C}{C_o} \times 100\% \qquad \textbf{(Equation 1)}$$

Where C_o is the initial concentration after 1 h dark reaction, C is the concentration of paracetamol after being treated with UV and visible light irradiation.

2.5 Optimization of pH Conditions for Photocatalytic Activity Testing

The photocatalytic activity testing was also conducted to optimize the pH value for BPA degradation (pHs of 2, 5, 7, 9), under visible light irradiation. BPA solution (25 ppm) was prepared, and the pH was adjusted using 0.05 M HCl for pH 2 and 0.05 M NaOH for pH 9 [17]. The photocatalytic experiment took place inside a light-shielded chamber equipped with a Philips 18 W

LED bulb. Before initiating the irradiation, the suspension was continuously stirred at ambient temperature in the dark for 1 h to establish equilibrium. Subsequently, the reaction proceeded under visible light exposure for 3.5 h. The photodegradation efficiency was determined using Equation 1.

3.0 Results and Discussion

3.1 Physicochemical Properties of MIL-100(Fe) and MIL-100(Fe)/TiO_2 Composites

3.1.1. Functional Group Analysis by FTIR Spectroscopy

The functional groups present in the prepared MIL-100(Fe)/TiO_2 materials were examined through FTIR spectroscopy, with the corresponding spectra displayed in Figure 2. A broad absorption band centred around 3468 cm^{-1} is associated with the stretching vibrations of hydroxyl (O–H) groups on the TiO_2 surface within both MIL-100(Fe)/TiO_2 samples [18]. However, this band appears more intense in MIL-100(Fe)/TiO_2 (5.4), indicating a higher concentration of hydroxyl groups, likely due to the increased TiO_2 content. These surface hydroxyl groups play a crucial role in photocatalysis by facilitating the generation of hydroxyl radicals [19]. Furthermore, a characteristic peak observed at 618 cm^{-1} is attributed to Ti–O stretching vibrations of the anatase phase, with its intensity increasing in line with the TiO_2 content [18].

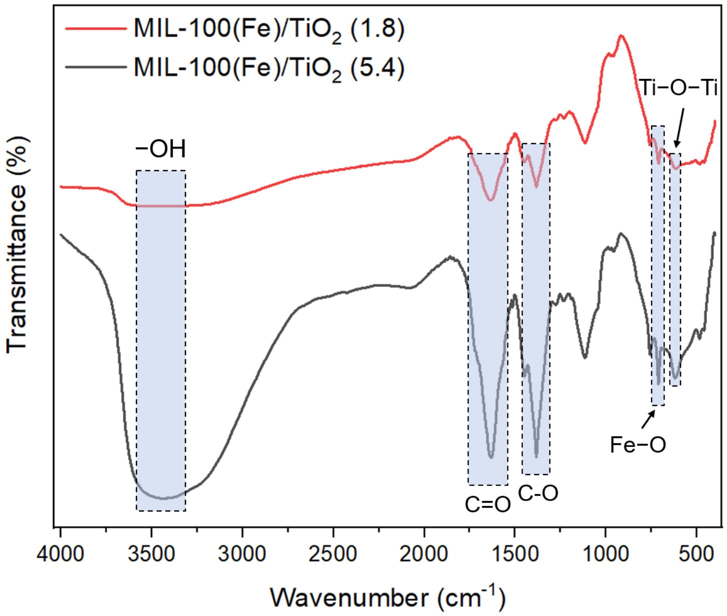

Figure 2: FTIR spectra of MIL-100(Fe)/TiO_2 (1.8) and MIL-100(Fe)/TiO_2 (5.4).

The FTIR spectra also reveal distinct absorption bands at 1416 cm^{-1} and 1636 cm^{-1}, which are attributed to the presence of carboxylic acid functionalities in MIL-100(Fe), specifically associated with the stretching vibrations of C−O and C=O bonds [20]. Moreover, a prominent signal at 715 cm^{-1} corresponds to the Fe–O within the iron-bound carboxylate groups, indicating that the structural integrity of MIL-100(Fe) has been retained [21]. These results indicate that TiO_2 was successfully modified with MIL-100(Fe) without disrupting the functional groups of TiO_2.

3.1.2. Bandgap Determination by Ultraviolet-visible-Near-Infrared (UV-vis-NIR) Spectroscopy

The optical behaviour of MIL-100(Fe) and its TiO_2-based composites was examined through UV-Vis absorption spectroscopy, as illustrated in Figure 3(a). MIL-100(Fe)/TiO_2 (1.8) and MIL-100(Fe)/TiO_2 (5.4) were compared alongside pure MIL-100(Fe). MIL-100(Fe) shows significant absorption within the visible spectrum, featuring a peak between 450 and 600 nm that reflects its capacity to utilize visible light. This characteristic band arises from the ligand-field 3*d*–3*d* transitions of Fe^{3+} ions present in the Fe_3O clusters of the MIL-100(Fe) framework [22].

With the addition of TiO_2, a noticeable redshift in the absorption edge occurs, indicating a shift toward longer wavelengths, indicating an extension of light absorption towards longer wavelengths. This shift implies that substantial electronic coupling occurs at the interface of MIL-100(Fe) and TiO_2, likely due to interfacial charge transfer mechanisms that modify the electronic configuration of the hybrid material [23]. The redshift intensifies with increasing TiO_2 content, reflecting enhanced charge transfer and electronic synergy at the MIL-100(Fe)/TiO_2 interface, resulting in stronger absorption of visible light [24]. The enhanced absorption across the visible spectrum indicates that the MIL-100(Fe)/TiO_2 composites are more effective at capturing light, a feature that could lead to improved efficiency in photocatalytic applications.

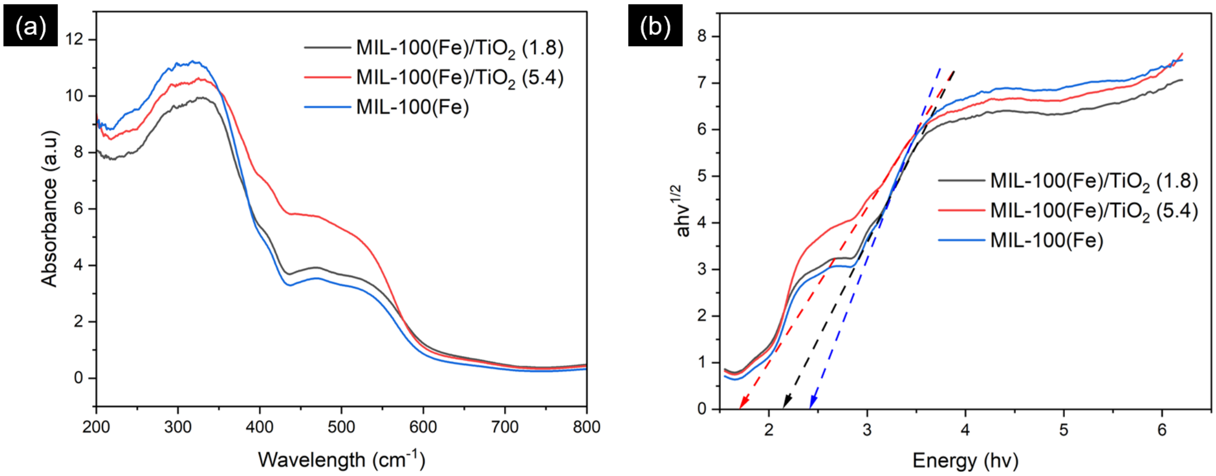

Figure 3: (a) Absorption spectra and (b) Tauc plot of the photocatalysts obtained by UV-vis-NIR spectroscopy.

The E_g of the photocatalysts was then determined by analyzing their UV-Vis-NIR absorption spectra. The Tauc plot method was employed to generate the graph of $(\alpha hv)^{1/2}$ versus energy (hv), and the E_g values were obtained through linear extrapolation at the x-intercept, as illustrated in Figure 3(b). Among all samples, MIL-100(Fe) demonstrated the highest E_g at 2.45 eV, whereas the introduction of TiO_2 led to a notable narrowing of the gap. Specifically, the E_g of MIL-100(Fe)/TiO_2 (1.8) was reduced to 2.10 eV, and further TiO_2 loading in MIL-100(Fe)/TiO_2 (5.4) caused an even more substantial decrease to 1.70 eV, reflecting increased responsiveness to visible light.

A further increase in the TiO_2 content leads to a more pronounced shift, as MIL-100(Fe)/TiO_2 (5.4) displays an even lower E_g of 1.70 eV, indicating enhanced visible-light absorption. Guesh *et al.* (2017) reported that Fe-based MOFs such as MIL-100(Fe) are well-suited for integration with semiconductors like TiO_2 due to their tunable electronic structures, narrow Eg, and high density of reactive sites. The synergy between these two materials enhances the separation of charge carriers, promotes the formation of bonding and antibonding molecular orbitals, and ultimately reduces the E_g, improving photocatalytic efficiency under visible-light irradiation [25].

3.1.3. Morphological Studies by Field Emission Scanning Electron Microscopy (FESEM)

Figure 4 illustrates the surface morphology of commercial TiO_2, MIL-100(Fe), and their corresponding composite materials. Figure 4(a) depicts the FESEM image of commercial TiO_2, which consists of small, nearly spherical nanoparticles that exhibit noticeable agglomeration. This agglomeration is a well-known phenomenon in TiO_2 due to its high surface energy, which induces strong van der Waals interactions among nanoparticles [26]. On the other hand, Figure 4(b) presents the morphology of MIL-100(Fe), which displays an irregular structure with sharp-edged particles and rough surfaces. These irregular structures suggest incomplete crystallization, leading to deviations from the well-defined octahedral geometry typically observed in MIL-100(Fe) [27].

Upon modification with MIL-100(Fe), Figure 4(c) shows the FESEM image of the MIL-100(Fe)/TiO_2 composites, where a noticeable distribution of TiO_2 interacting with the rough textured surface of MIL-100(Fe). The small TiO_2 nanoparticles adhere to the larger MIL-100(Fe) structures, suggesting enhanced surface area and dispersion [24]. As the TiO_2 content increases, the morphology becomes more compact and dense (Figure 4(d)). The MIL-100(Fe) framework appears increasingly embedded within the TiO_2 network, forming larger agglomerates. This phenomenon is likely due to the strong interaction between the two components, leading to a more uniform composite structure.

The average particle sizes of the photocatalysts are shown in Table 2. The increment of TiO_2 content within the MIL-100(Fe)/TiO_2 composites leads to a significant enlargement in particle size. Specifically, the MIL-100(Fe)/TiO_2 (1.8) exhibits an average particle size of 54.7 nm, which rises to 74.7 nm in the MIL-100(Fe)/TiO_2 (5.4). This trend indicates that TiO_2 particles contribute to the overall particle size of the composite, possibly due to surface coverage and the formation of larger agglomerates [24].

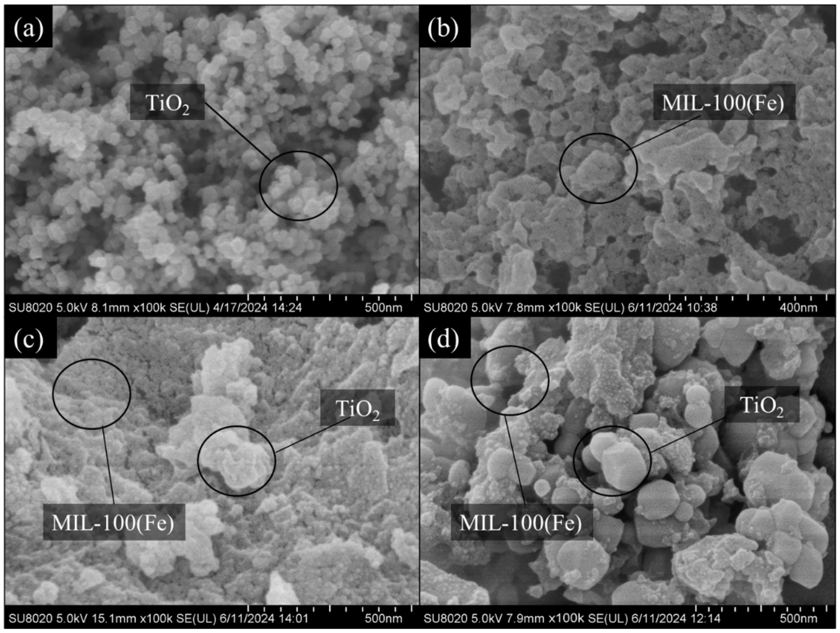

Figure 4: FESEM images of (a) commercial TiO_2, (b) MIL-100(Fe), (c) MIL-100(Fe)/TiO_2 (1.8), and (d) MIL-100(Fe)/TiO_2 (5.4).

Elemental composition and distribution of the synthesized MIL-100(Fe)/TiO_2 composites were examined through energy dispersive X-ray (EDX) analysis, verifying their successful synthesis. The EDX analysis data are presented in Figure 5. The synthesized materials primarily consist of carbon (C), oxygen (O), iron (Fe), and titanium (Ti). Small amounts of chlorine (Cl) and sodium (Na) are also detected, which are likely residuals from the precursor materials used during synthesis.

Table 2: Average particle size of the photocatalysts

Photocatalysts	Average particle sizes (nm)
Commercial TiO_2	49.8
MIL-100(Fe)	52.6
MIL-100(Fe)/TiO_2 (1.8)	54.7
MIL-100(Fe)/TiO_2 (5.4)	74.7

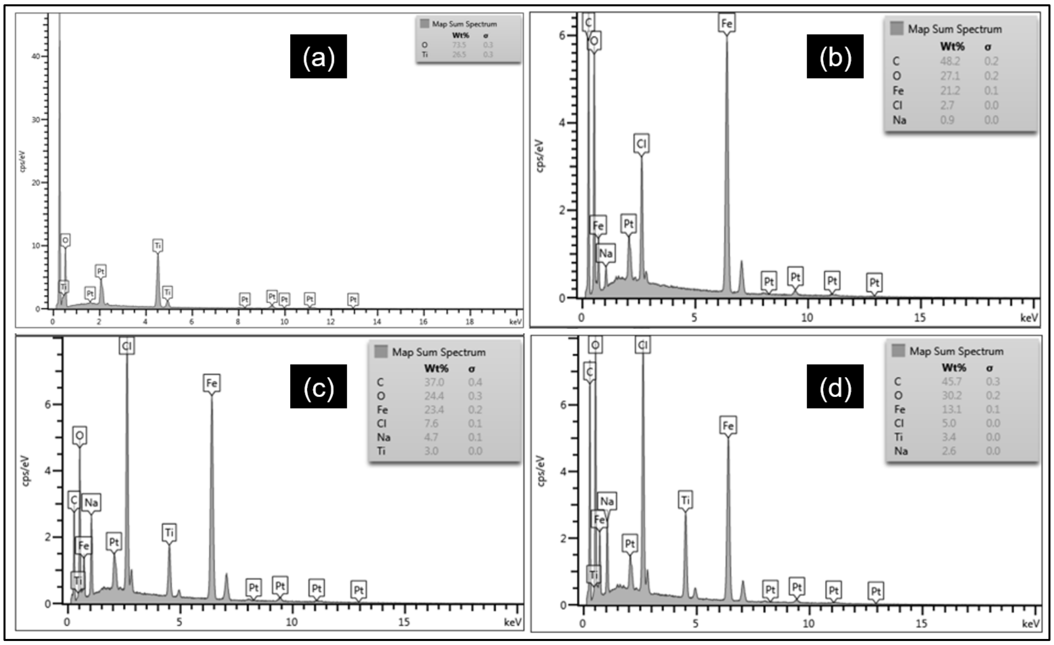

Figure 5: EDX spectra of (a) commercial TiO_2, (b) MIL-100(Fe), (c) MIL-100(Fe)/TiO_2 (1.8) and (d) MIL-100(Fe)/TiO_2 (5.4).

Table 3: Atomic compositions of the photocatalysts

Samples	**Atomic Ratio (%)**			
	C	**O**	**Fe**	**Ti**
Commercial TiO_2	-	82.9	-	17.1
MIL-100(Fe)	48.2	27.1	21.2	-
MIL-100(Fe)/TiO_2 (1.8)	37.0	24.4	23.4	3.0
MIL-100(Fe)/TiO_2 (5.4)	45.7	30.2	13.1	3.4

Table 3 lists the atomic composition of the elements identified in the MIL-100(Fe)/TiO_2 composites based on EDX analysis. Carbon was the most abundant element detected in all samples, primarily due to the intrinsic structure of MIL-100(Fe), which contains organic linkers rich in carbon. The percentage of Ti and O species varied between samples, reflecting the different amounts of TiO_2 incorporated. A higher amount of TiO_2 led to a greater presence of titanium and oxygen elements, with MIL-100(Fe)/TiO_2 (5.4) exhibiting higher Ti and O content than MIL-100(Fe)/TiO_2 (1.8). The presence of Fe species, which is derived from the MIL-100(Fe) structure, was consistent across all samples. However, impurities were also observed in all samples. The Pt peaks detected in the spectra are due to the Pt coating applied before FESEM and EDX analysis, which was intended to enhance the imaging quality [28].

3.1.4. Crystallinity by X-Ray Diffraction (XRD)

The XRD diffractogram of MIL-100(Fe), MIL-100(Fe)/TiO_2 (1.8), and MIL-100(Fe)/TiO_2 (5.4) composites are illustrated in Figure 6. The diffractogram for the MIL-100(Fe) composites (Figure 6(a)) reveals the characteristic peaks at 2θ values of 11.00°, 20.20°, 25.58°, and 27.58°, corresponding to the (003), (101), (012), and (104) planes, respectively, as documented in JCPDS 01-075-2553. These peaks confirm the MIL-100(Fe)'s crystal structure, indicating its low crystallinity and partially amorphous characteristics, which are typical for Fe_3BTC materials due to the low synthesis temperature employed [29].

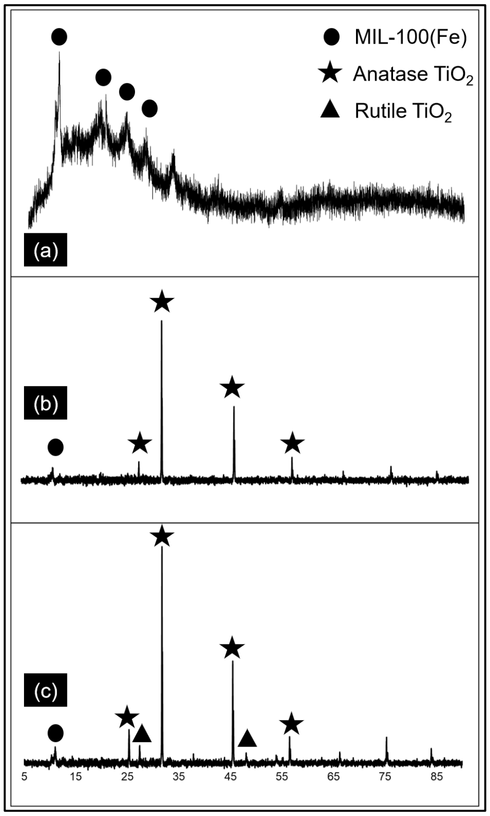

Figure 6: XRD diffractogram of (a) MIL-100(Fe), (b) MIL-100(Fe)/TiO_2 (1.8), (c) MIL-100(Fe)/TiO_2 (5.4)

The diffraction patterns of all prepared MIL-100(Fe)/TiO_2 composites reveal distinct peaks attributable to both the MIL-100(Fe) framework and TiO_2 crystalline phases. Notably, for MIL-100(Fe)/TiO_2 (1.8) (Figure 6(b)), the formation of peaks at 2θ values of 25.26°, 32.48°, 45.75°, and 56.89° are observed, corresponding to the (101), (200), (210), and (211) planes of anatase TiO_2. However, no peaks corresponding to the rutile phase are detected, which may be attributed to the low amount of TiO_2

[30]. As the amount of TiO_2 increases, the spectra show peaks characteristic of both anatase and rutile phases as depicted in Figure 6(c). Peaks at 27.12° and 35.75°, corresponding to the (110) and (101) planes of the rutile phase, are also detected, as indexed in ICDD 01-076-1941. This suggests the simultaneous presence of both rutile and anatase TiO_2 phases within the composite, particularly in samples with elevated TiO_2 content [30].

Furthermore, the peak intensity at $2\theta = 25.26°$ becomes more pronounced, signifying an enhanced degree of crystallinity and an increased number of atoms in the crystal lattice [31]. The characteristic peak of MIL-100(Fe) at 2θ value of 10.3° remains present in both composites, confirming that MIL-100(Fe) has been effectively integrated onto the TiO_2 matrix while maintaining its original structural characteristics.

3.2 Photocatalytic Testing

The determination of the photocatalytic efficacy of the synthesized photocatalysts is an essential component of the photodegradation study. BPA was employed as a model organic pollutant to examine the photocatalytic performance of commercial TiO_2 and MIL-100(Fe)/TiO_2 composites containing different TiO_2 loadings (1.8, 3.6, 5.4, and 7.2 mmol) under ultraviolet light irradiation. Variations in the percentage of photodegradation of BPA were anticipated depending on the amount of TiO_2.

Figure 7 illustrates the degradation percentage of BPA using the synthesized photocatalysts after 3.5 h of UV light irradiation. In the absence of a photocatalyst (photolysis), a low BPA degradation of 21.06% was observed. This is due to the fact that BPA degradation occurs mainly through direct UV light absorption by the molecule, which is less effective, confirming the need for photocatalysts to significantly enhance BPA degradation [32]. Among the MIL-100(Fe)/TiO_2 photocatalysts, MIL-100(Fe)/TiO_2 (5.4) achieved the highest degradation percentage of 81.43%, while MIL-100(Fe)/TiO_2 (1.8) showed the lowest degradation at 36.36%.

The correlation between the TiO_2 content in the MIL-100(Fe)-modified TiO_2 photocatalysts and their photocatalytic performance is evident. Raising the TiO_2 content to 5.4 mmol significantly enhanced the photocatalytic performance, likely due to the synergistic effect between MIL-100(Fe) and TiO_2 [33]. This interaction enhances both light-harvesting capability and the separation of photogenerated charge carriers, thereby improving overall photocatalytic activity. However, further increasing the TiO_2 content to 7.2 mmol reduced the photocatalytic efficiency to 62.16%. This decline could be attributed to excessive TiO_2 loading, which may hinder light penetration and reduce the availability of active sites for photocatalysis [7]. Hence, these findings indicate that the optimum TiO_2 content for MIL-100(Fe)/TiO_2 composites is 5.4 mmol, as it provides a balance between sufficient active sites, enhanced light absorption, and efficient charge separation. Beyond this amount, the negative effects of excessive TiO_2 loading outweigh the benefits, leading to a decrease in photocatalytic performance [24].

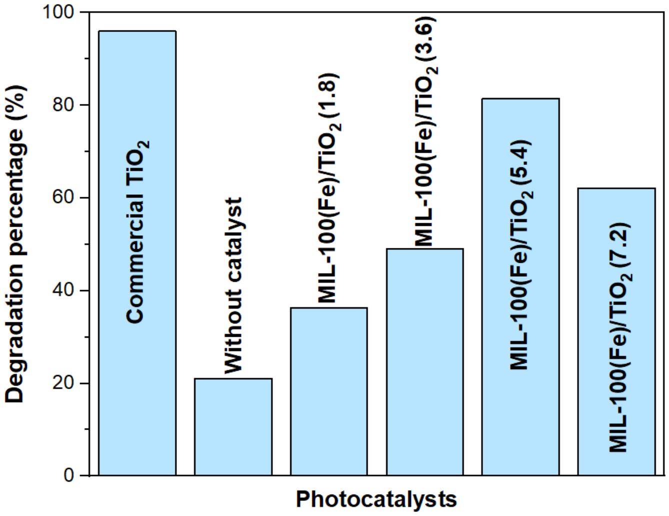

Figure 7: Degradation percentage of BPA under UV light irradiation in the presence of different photocatalysts. Experiment condition: addition of photocatalyst (0.05 g) in BPA (25 ppm) and reaction time of 3.5 h.

Moreover, commercial TiO_2 demonstrated an impressive degradation efficiency of 96.02%, surpassing the performance of all synthesized photocatalysts. Despite the modification with MIL-100(Fe), TiO_2 remains the primary active component in the composite. TiO_2 is known to be highly effective under UV light, but its wide E_g limits its activity in the visible light range, which accounts for a significantly higher fraction of solar energy [5]. In order to evaluate the photocatalysts' performance in visible light, the degradation of BPA was measured using commercial TiO_2 and MIL-100(Fe)/TiO_2 composites containing the optimal TiO_2 content (5.4 mmol) under visible light irradiation. This experiment aimed to assess the efficacy of the photocatalysts under visible light irradiation. The BPA degradation percentages after 3.5 h of visible light irradiation are presented in Figure 8.

The results revealed that MIL-100(Fe)/TiO_2 (5.4) attained a significant degradation efficiency of 69.49%, while commercial TiO_2 showed no detectable degradation. Under visible light irradiation, TiO_2 is unable to generate the electron-hole pairs required for photocatalysis [34]. TiO_2's wide E_g restricts its ability to effectively absorb visible light, which in turn limits its photocatalytic performance under such illumination. On the other hand, the enhanced degradation efficacy observed in the MIL-100(Fe)/TiO_2 composites due to the Fe–O clusters within the MIL-100(Fe) framework, which are directly responsive to visible light activation [35]. This excitation facilitates the generation of charge carriers, enabling photocatalytic reactions. Furthermore, the MIL-100(Fe) framework enhances charge separation, as the Fe centers serve as sites that suppress electron-hole recombination, prolonging charge carrier lifetimes [36]. This feature promotes stronger interactions between the pollutants and the photocatalysts.

Building on these results, the role of pH in BPA degradation was examined, as it significantly influences photocatalytic activity. Changes in pH can influence the surface charge of the photocatalyst, thereby impacting the efficiency of charge migration during the reaction. The following section explores how varying pH levels affect the photodegradation performance of the MIL-100(Fe)/TiO_2 composites.

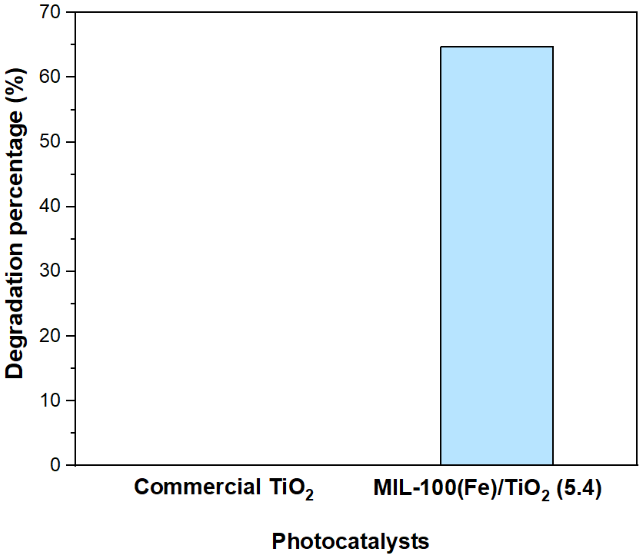

Figure 8: Percentage of BPA degradation under visible light exposure utilizing commercial TiO_2 and MIL-100(Fe)/TiO_2 (5.4). Experiment condition: addition of photocatalyst (0.05 g) in BPA (25 ppm) and reaction time of 3.5 h.

3.3 Photocatalytic Activity pH Optimization of MIL-100(Fe)/TiO_2 Composites in the Photodegradation of BPA

The photocatalytic activity of MIL-100(Fe)/TiO_2 (5.4) was further tested at various pH levels (2, 5, 7, and 9) to determine the optimal pH condition for BPA degradation under visible light exposure. Figure 9 presents the percentage of BPA degradation after 3.5 h of irradiation. The results indicate that the highest degradation occurred at pH 2 (95.71%), highlighting the significant influence of pH on the photocatalytic process.

At pH 2, the TiO_2 surface experiences an excess of H^+ ions, which can hinder the reaction by causing TiO_2 aggregation [37]. This aggregation reduces the active surface area of the photocatalyst. The combination of MIL-100(Fe) and TiO_2 in the composite improves charge carrier separation, reducing the effects of particle aggregation and increasing the overall photocatalytic efficiency by suppressing electron-hole recombination [38]. The acidic environment at pH 2 also promotes enhanced electron-hole formation, leading to increased anion adsorption and contributing to higher degradation efficiency. As a result, the highest BPA degradation efficiency of 97.56% was achieved at this pH.

In comparison, at pH 5 and 7, the degradation efficiencies decreased to 81.14% and 91.21%, respectively. At these near-neutral pH values, TiO_2 maintains a balance between positive and negative surface charges, which impacts the adsorption of anions and the efficiency of charge separation [39]. This equilibrium creates less optimal conditions for the photocatalytic reaction, resulting in a lower degradation efficiency compared to that observed at pH 2. At pH 9, the TiO_2 surface becomes negatively charged, which reduces anion adsorption due to repulsion between the surface and the anions, resulting in a degradation efficiency of 83.93%. Although this efficiency is lower than at pH 2 and 7, the efficiency remains higher than at pH

5, indicating that the bonding between MIL-100(Fe) and TiO_2 contributes to sustaining photocatalytic performance even at alkaline conditions [40]. Therefore, pH 2 was determined as the optimal condition for BPA degradation using MIL-100(Fe)/TiO_2, achieving the highest degradation percentage.

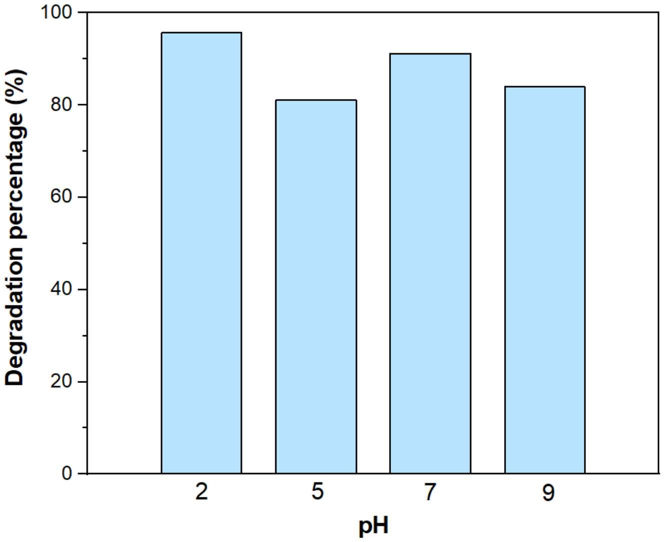

Figure 9: Degradation percentage of BPA under visible light irradiation in the presence of MIL-100(Fe)/TiO_2 (5.4) with different pH. Experiment condition: photocatalyst (0.05 g) was added to BPA with different pHs and a reaction time of 3.5 h.

4.0 Conclusion

This study successfully synthesized MIL-100(Fe)/TiO_2 composites through the hydrothermal method with varying TiO_2 content. Characterization techniques including FTIR, XRD, FESEM-EDX, and UV-vis-NIR spectroscopy verified the effective integration of MIL-100(Fe) onto the TiO_2 matrix, preserving the anatase crystalline phase while inducing distinct structural and optical alterations. The presence of MIL-100(Fe) influenced the crystalline structure of the composites, surface morphology, and their ability to absorb light. The MIL-100(Fe)/TiO_2 (5.4) composite demonstrated superior photocatalytic performance, achieving 81.43% BPA degradation under UV light, attributed to its optimized TiO_2 content, improved charge separation, and enhanced light absorption. Under visible light exposure, the same composite retained significant photocatalytic effectiveness (69.49%), whereas commercial TiO_2 showed negligible activity, a difference credited to the Fe–O clusters within MIL-100(Fe) promoting visible light absorption and enhanced electron mobility. pH optimization studies revealed that MIL-100(Fe)/TiO_2 (5.4 mmol) exhibited the highest degradation efficiency (95.71%) at pH 2, suggesting that acidic conditions favor charge separation and pollutant adsorption. Thus, the synthesized MIL-100(Fe)/TiO_2 composites demonstrated promising photocatalytic performance under both UV and visible light, with optimal activity at acidic pH. These findings emphasize their potential applicability aimed at degrading organic contaminants.

Acknowledgment

The authors gratefully acknowledge funding provided by Universiti Teknologi Malaysia from Geran Penyelidikan Hi-Tech (F4) (Q.J130000.4654.00Q19) and PDRU Grant Vote No. 07E44.

References

1. Farooq, N., Kallem, P., ur Rehman, Z., Imran Khan, M., Kumar Gupta, R., Tahseen, T., Mushtaq, Z., Ejaz, N., & Shanableh, A. (2024). Recent trends of titania (TiO_2) based materials: A review on synthetic approaches and potential applications. Journal of King Saud University - Science, 36(6), 103210.
2. Eddy, D. R., Permana, M. D., Sakti, L. K., Sheha, G. A. N., Solihudin, Hidayat, S., Takei, T., Kumada, N., & Rahayu, I. (2023). Heterophase polymorph of TiO_2 (anatase, rutile, brookite, TiO_2(B)) for efficient photocatalyst: Fabrication and activity. Nanomaterials, 13(4), 704.
3. Thakur, N., Kumar, A., Thakur, V. K., Kalia, S., Arya, V., Kumar, A., Kumar, S., & Kyzas, G. Z. (2024). A critical review on the recent trends of photocatalytic, antibacterial, antioxidant and nanohybrid applications of anatase and rutile TiO_2 nanoparticles. Science of The Total Environment, 914, 169815.
4. Zhou, H., Wang, H., Yue, C., He, L., Li, H., Zhang, H., Yang, S., & Ma, T. (2024). Photocatalytic degradation by TiO_2-conjugated/coordination polymer heterojunction: Preparation, mechanisms, and prospects. Applied Catalysis B: Environment and Energy, 344, 123605.

5. Thoda, O., Moschovi, A. M., Sakkas, K. M., Polyzou, E., & Yakoumis, I. (2023). Highly active under VIS light M/TiO_2 photocatalysts prepared by single-step synthesis. Applied Sciences, 13.
6. Guo, J., Gan, W., Chen, R., Zhang, M., & Sun, Z. (2023). Au nanoparticle sensitized blue TiO_2 nanorod arrays for efficient Gatifloxacin photodegradation. RSC Advances, 13(40), 28299–28306.
7. Sultana, M., Marzia, A., Islam, S., Khatun, M. A., Rahaman, M. H., Chakraborty, A. K., Rahman, M. S., Rahman, M. M., & Nur, A. S. M. (2023). Strategic development of metal doped TiO_2 photocatalysts for enhanced dye degradation activity under UV–Vis irradiation: A review. Current Research in Green and Sustainable Chemistry, 7, 100383.
8. Geldasa, F. T., Kebede, M. A., Hone, F. G., & Jira, E. T. (2024). Influence of non-metals doping on the structural, electronic, optical, and photocatalytic properties of rutile TiO_2 based on density functional theory computations. Computational Condensed Matter, 41, e00970.
9. Fard, N. E., Ali, N. S., Saady, N. M. C., Albayati, T. M., Salih, I. K., Zendehboudi, S., Harharah, H. N., & Harharah, R. H. (2024). A review on development and modification strategies of MOFs Z-scheme heterojunction for photocatalytic wastewater treatment, water splitting, and DFT calculations. Heliyon, 10(13), e32861.
10. Zhu, Y., Zhou, S., Zhu, J., Wang, P., Wang, X., Jia, X., Wågberg, T., & Hu, G. (2022). Mesoporous carbon decorated with MIL-100(Fe) as an electrochemical platform for ultrasensitive determination of trace cadmium and lead ions in surface water. Ecotoxicology and Environmental Safety, 243, 113987.
11. Hejazi, R., Mahjoub, A. R., Khavar, A. H. C., & Khazaee, Z. (2020). Fabrication of novel type visible-light-driven TiO_2@MIL-100(Fe) microspheres with high photocatalytic performance for removal of organic pollutants. Journal of Photochemistry and Photobiology A: Chemistry, 400, 112644.
12. Channab, B.-E., El Ouardi, M., Ait Layachi, O., Marrane, S. E., El Idrissi, A., BaQais, A., & Ait Ahsaine, H. (2023). Recent trends on MIL-Fe metal–organic frameworks: Synthesis approaches, structural insights, and applications in organic pollutant adsorption and photocatalytic degradation. Environmental Science: Nano, 10(11), 2957–2988.
13. Razia, S., Hadibarata, T., & Lau, S. Y. (2024). A review on biodegradation of Bisphenol A (BPA) with bacteria and fungi under laboratory conditions. International Biodeterioration & Biodegradation, 195, 105893.
14. Abu Hasan, H., Muhamad, M. H., Budi Kurniawan, S., Buhari, J., & Husain Abuzeyad, O. (2023). Managing Bisphenol A contamination: Advances in removal technologies and future prospects. Water, 15(20), 3573.
15. Lestari, W. W., Yunita, L., Saraswati, T. E., Heraldy, E., Khafidhin, M. A., Krisnandi, Y. K., Arrozi, U. S. F., & Kadja, G. T. M. (2021). Fabrication of composite materials MIL-100(Fe)/Indonesian activated natural zeolite as enhanced CO_2 capture material. Chemical Papers, 75(7), 3253–3263.
16. Rojas-Guerrero, C., Villanueva-Rodríguez, M., Guzmán-Mar, J., Hernández-Ramírez, A., Cedillo-González, E., Rodríguez, F. L., & Hinojosa-Reyes, L. (2023). Evaluation of the applicability of the TiO_2/MIL-100(Fe) composite material. Journal of Environmental Chemical Engineering, 11(5), 110415.
17. Wardhani, S., Purwonugroho, D., Fitri, C. W., & Prananto, Y. P. (2018). Effect of pH and irradiation time on TiO_2-chitosan activity for phenol photo-degradation. AIP Conference Proceedings, 2021(1), 050009.
18. Sadek, O., Touhtouh, S., Rkhis, M., & Hajjaji, A. (2024). Study of the hydroxylation of the TiO_2 thin layer prepared by spin-coating method using FTIR analysis and DFT theory. Inorganic Chemistry Communications, 161, 112092.
19. Hwang, J. Y., Moon, G., Kim, B., Tachikawa, T., Majima, T., Hong, S., Cho, K., Kim, W., & Choi, W. (2021). Crystal phase-dependent generation of mobile OH radicals on TiO_2: Revisiting the photocatalytic oxidation mechanism of anatase and rutile. Applied Catalysis B: Environment and Energy, 286, 119905.
20. Nehra, M., Dilbaghi, N., Singhal, N. K., Hassan, A. A., Kim, K.-H., & Kumar, S. (2019). Metal-organic frameworks MIL-100(Fe) as an efficient adsorptive material for phosphate management. Environmental Research, 169, 229–236.
21. Lomba-Fernández, B., Fdez-Sanromán, A., Pazos, M., Sanromán, M. A., & Rosales, E. (2024). Iron metal-organic framework nanofiber membrane for the integration of electro-Fenton and effective continuous treatment of pharmaceuticals in water. Chemosphere, 366, 143447.
22. Wu, W., Zhu, J., Deng, Y., Xiang, Y., Tan, Y., Tang, H., Zou, H., Xu, Y., & Zhou, Y. (2019). TiO_2 nanocrystals with the {001} and {101} facets co-exposed with MIL-100(Fe): An egg-like composite nanomaterial for efficient visible light-driven photocatalysis. RSC Advances, 9, 31728–31734.
23. Sheraz, M., & Kim, J. (2024). Reusable MIL-100(Fe)-polyacrylonitrile-TiO_2 nanofiber webs for adsorption and decomposition of toluene. Chemical Engineering Journal, 496, 153542.
24. Huang, C.-W., Zhou, S.-R., & Hsiao, W.-C. (2024). Multifunctional TiO_2/MIL-100(Fe) to conduct adsorption, photocatalytic, and heterogeneous photo-Fenton reactions for removing organic dyes. Journal of the Taiwan Institute of Chemical Engineers, 158, 104850.
25. Guesh, K., Caiuby, C. A. D., Mayoral, Á., Díaz-García, M., Díaz, I., & Sanchez-Sanchez, M. (2017). Sustainable preparation of MIL-100(Fe) and its photocatalytic behavior in the degradation of methyl orange in water. Crystal Growth & Design, 17(4), 1806–1813.

26. Janczarek, M., Klapiszewski, Ł., Jędrzejczak, P., Klapiszewska, I., Ślosarczyk, A., & Jesionowski, T. (2022). Progress of functionalized TiO_2-based nanomaterials in the construction industry: A comprehensive review. Chemical Engineering Journal, 430, 132062.
27. Elharony, N., Sayed, I., Al-sehemi, A., Al-Ghamdi, A., & Abou Elyazed, A. (2021). Facile synthesis of iron-based MOFs MIL-100(Fe) as heterogeneous catalyst in Kabachnick reaction. Catalysts, 11, 1451.
28. Erdman, N., Bell, D. C., & Reichelt, R. (2019). Scanning electron microscopy. In P. W. Hawkes & J. C. H. Spence (Eds.), Springer Handbook of Microscopy (pp. 229–318). Springer International Publishing.
29. Li, L., Xu, S., Liu, Z., & Wang, D. (2024). Insight into the growth mechanism of low-temperature synthesis of high-purity lithium slag-based zeolite A. Materials, 17(3), 568
30. Belekoukia, M., Tan, J., Andresen, J., Wang, H., Maroto-Valer, M., & Xuan, J. (2019). Laser induced plasmonic heating with Au-decorated TiO_2 nanoparticles. Energy Procedia, 158, 5647–5652.
31. Al-Baradi, A. M., Al-Shehri, S. F., Badawi, A., Merazga, A., & Atta, A. A. (2018). A study of optical, mechanical and electrical properties of poly(methacrylic acid)/TiO_2 nanocomposite. Results in Physics, 9, 879–885.
32. Ghosh, S., Pourebrahimi, S., Malloum, A., Ajala, O. J., AlKafaas, S. S., Onyeaka, H., Nnaji, N. D., Oroke, A., Bornman, C., Christian, O., Ahmadi, S., & Wani, M. Y. (2023). A review on ciprofloxacin removal from wastewater as a pharmaceutical contaminant: Covering adsorption to advanced oxidation processes to computational studies. Materials Today Communications, 37, 107500.
33. He, X., Fang, H., Gosztola, D. J., Jiang, Z., Jena, P., & Wang, W.-N. (2019). Mechanistic insight into photocatalytic pathways of MIL-100(Fe)/TiO_2 composites. ACS Applied Materials & Interfaces, 11(13), 12516–12524.
34. Le, T. M., & Nguyen, T. D. (2024). Enhancement of visible-light photocatalysis of TiO_2 via nanocomposite incorporating with Fe(III) species. Results in Engineering, 23, 102500.
35. Yi, H., Jiang, M., Huang, D., Zeng, G., Lai, C., Qin, L., Zhou, C., Li, B., Liu, X., Cheng, M., Xue, W., Xu, P., & Zhang, C. (2018). Advanced photocatalytic Fenton-like process over biomimetic hemin-Bi_2WO_6 with enhanced pH. Journal of the Taiwan Institute of Chemical Engineers, 93, 184–192.
36. Wei, Y., Fu, Z., Meng, Y., Li, C., Yin, F., Wang, X., Zhang, C., Guo, L., & Sun, S. (2024). Photocatalytic degradation of methylene blue over MIL-100(Fe)/GO composites: A performance and kinetic study. International Journal of Coal Science & Technology, 11(1), 42.
37. Rosa, D., Manetta, G., & Di Palma, L. (2024). Experimental assessment of the pH effect and ions on the photocatalytic activity of iron-doped titanium dioxide supported on polystyrene pellets: Batch and continuous tests. Chemical Engineering Science, 291, 119918.
38. Lee, H., Lee, H., Ahn, S., & Kim, J. (2022). MIL-100(Fe)-hybridized nanofibers for adsorption and visible light photocatalytic degradation of water pollutants: Experimental and DFT approach. ACS Omega, 7(24), 21145–21155.
39. Nasikhudin, Diantoro, M., Kusumaatmaja, A., & Triyana, K. (2018). Study on photocatalytic properties of TiO_2 nanoparticle in various pH condition. Journal of Physics: Conference Series, 1011(1), 012069.
40. Kisała, J., Hörner, G., Barylyak, A., Pogocki, D., & Bobitski, Y. (2022). Photocatalytic degradation of 4,4′-isopropylidenebis(2,6-dibromophenol) on sulfur-doped nano TiO_2. Materials, 15(1), 361.